Electronic Supplementary Information (ESI)

The annual-hydrogen-yield-climatic-response ratio: evaluating the real-life performance of integrated solar water splitting devices

Moritz Kölbach,[*a,b,c] Oliver Höhn,[d] Kira Rehfeld,[e] Manuel Finkbeiner,[f] James Barry,[f,g] and Matthias M. May[a,b]

[a]Universität Tübingen, Institute of Physical and Theoretical Chemistry, Tübingen, Germany.
[b]Universität Ulm, Institute of Theoretical Chemistry, Ulm, Germany.
[c]Helmholtz-Zentrum Berlin für Materialien und Energie GmbH, Institute for Solar Fuels, Berlin, Germany.
[d]Fraunhofer ISE für Solare Energiesysteme, Freiburg, Germany.
[e]Universität Tübingen, Department of Geosciences and Department of Physics, Tübingen, Germany.
[f]Universität Heidelberg, Institute of Environmental Physics, Heidelberg, Germany.
[g]International Centre for Sustainable Development, Hochschule Bonn-Rhein-Sieg, Sankt Augustin, Germany.

[*]Email Address: moritz.koelbach@uni-tuebingen.de

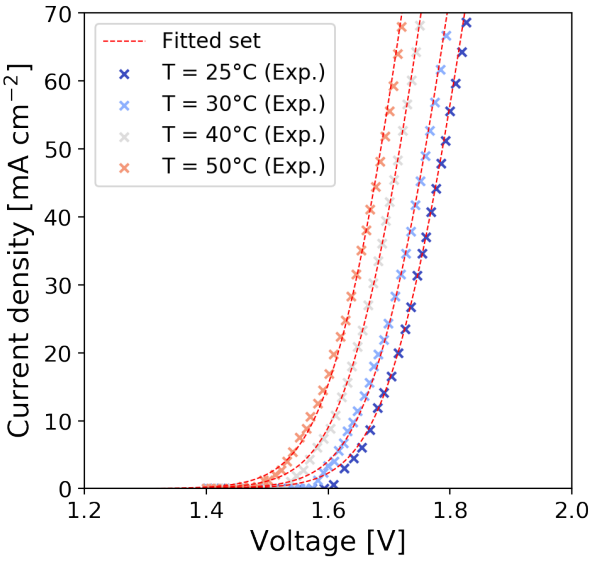

Fig. S1: Fitted set of temperature-dependent experimental IV curves of an AEM electrolyzer[1] using the routine described in the manuscript.

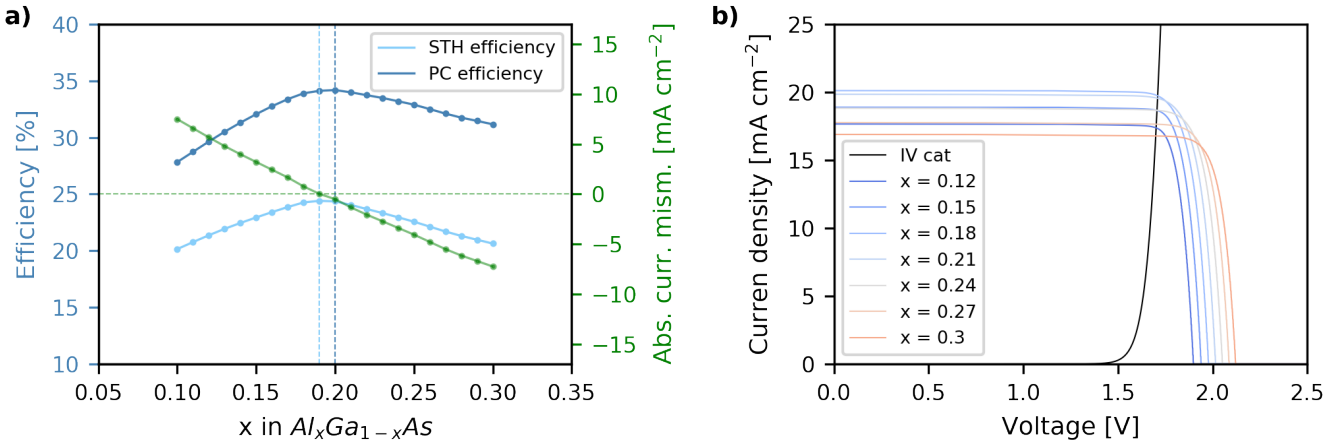

Fig. S2: (a) Left y-axis: STH and photoconversion (PC) efficiency as a function of the x in the $Al_xGa_{1-x}As$ top absorber for a device operating temperature of 25°C under AM1.5g illumination. The efficiency maxima are indicated as vertical dashed lines. Right y-axis: Corresponding absolute current mismatch in the dual-junction. (b) Corresponding IV characteristics of the AEM electrolyzer and the solar cell for exemplary top absorber compositions.

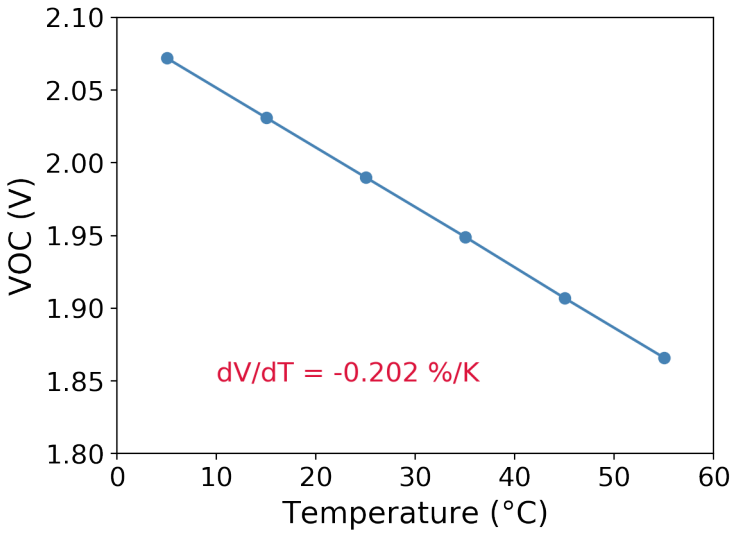

Fig. S3: Modelled open circuit voltage of the AlGaAs//Si dual-junction as a function of the temperature. A VOC temperature coefficient of -0.202 %/K can be extracted.

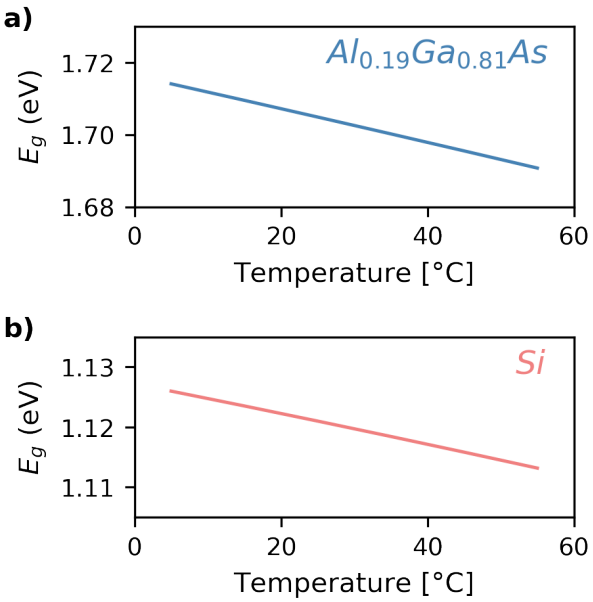

Fig. S4: Temperature dependence of the bandgap of (a) AlGaAs and (b) Si.

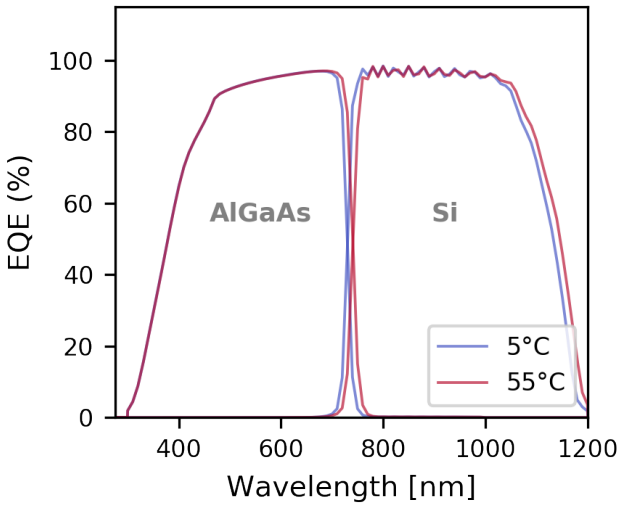

Fig. S5: Modelled external quantum efficiency of the AlGaAs top and Si bottom absorber for a temperature of 5°C and 55°C assuming an incidence angle of 0°.

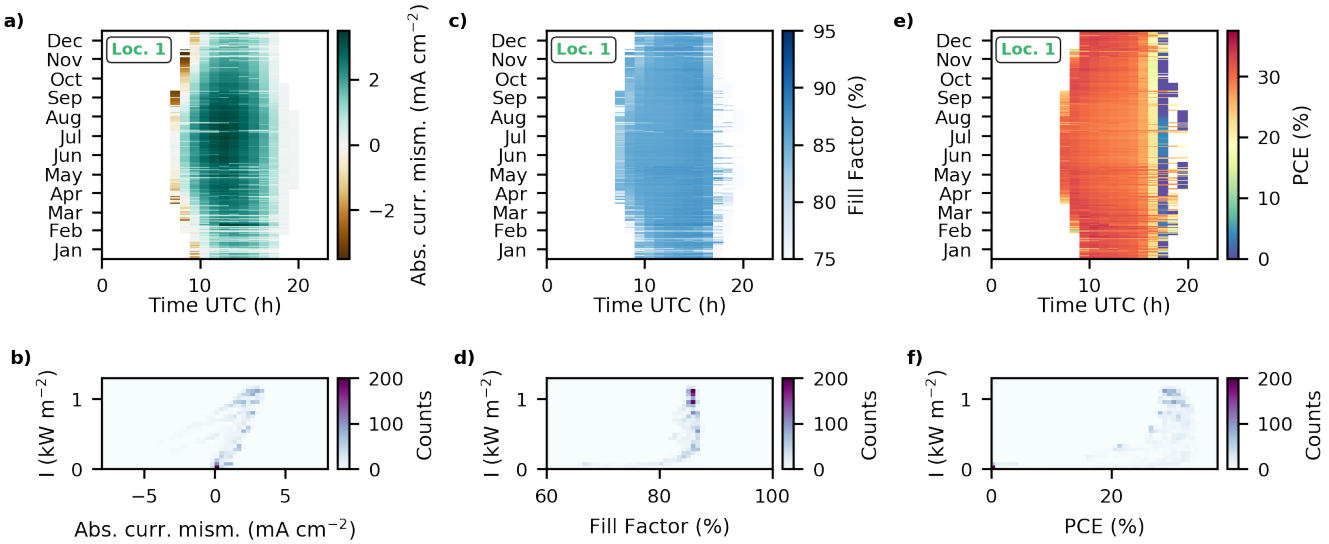

Fig. S6: Modelled climatic response of the AlGaAs//Si dual-junction for the location in southern California. (a) Hourly resolved annual absolute current mismatch in the dual-junction. (b) 2D histogram of the absolute current mismatch with regard to the total spectral irradiance impinging on the device. (c) Hourly resolved annual fill factor of the dual-junction. (d) 2D histogram of the fill factor and the total spectral irradiance. (d) Hourly resolved annual photoconversion efficiency (PCE). (e) 2D histogram of the PCE and the total spectral irradiance.

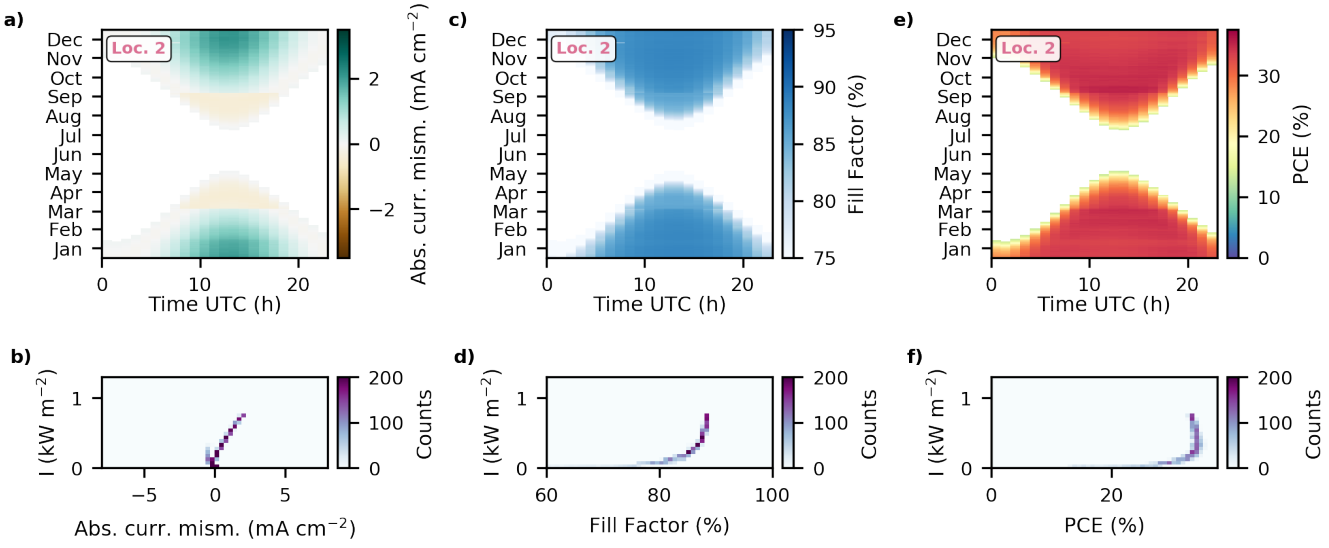

Fig. S7: Modelled climatic response of the AlGaAs//Si dual-junction in Antarctica. (a) Hourly resolved annual absolute current mismatch in the dual-junction. (b) 2D histogram of the absolute current mismatch with regard to the total spectral irradiance impinging on the device. (c) Hourly resolved annual fill factor of the dual-junction. (d) 2D histogram of the fill factor and the total spectral irradiance. (d) Hourly resolved annual PCE. (e) 2D histogram of the PEC and the total spectral irradiance.

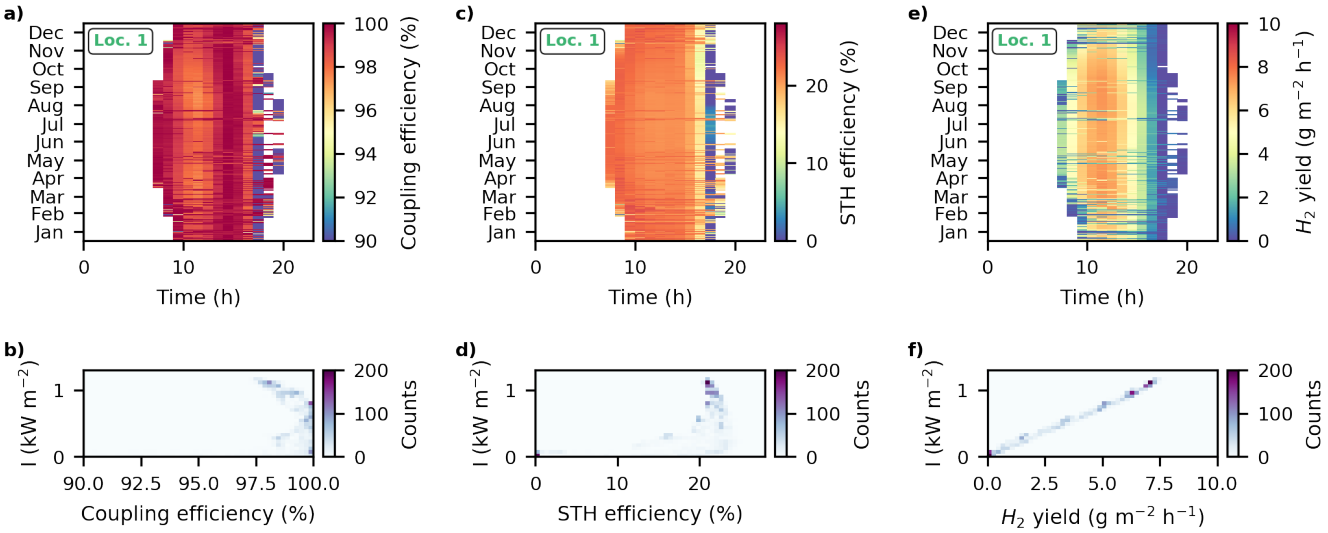

Fig. S8: Modelled climatic response of the solar water splitting device based on an AlGaAs//Si dual-junction and an AEM electrolyzer for the location in southern California for a thermally decoupled configuration. (a) Hourly resolved annual coupling efficiency. (b) 2D histogram of the coupling efficiency with regard to the total spectral irradiance impinging on the device. (c) Hourly resolved annual STH efficiency. (d) 2D histogram of the STH efficiency and the total spectral irradiance. (d) Hourly resolved annual hydrogen yield. (e) 2D histogram of the hydrogen yield and the total spectral irradiance.

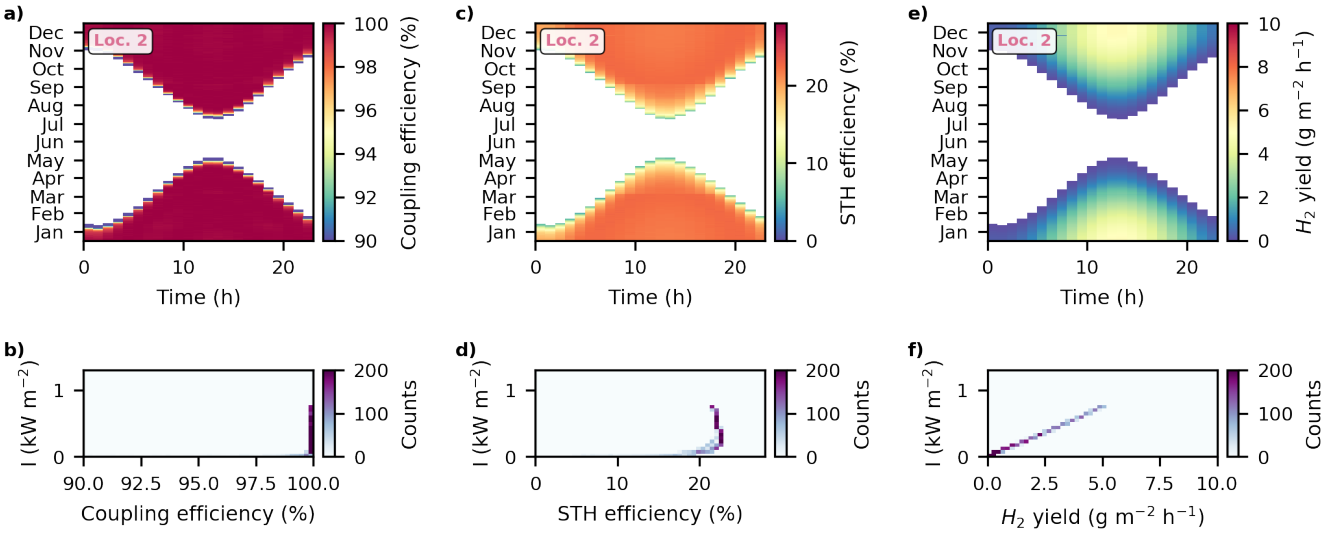

Fig. S9: Modelled climatic response of the solar water splitting device based on an AlGaAs//Si dual-junction and an AEM electrolyzer for the location in Antarctica for a thermally decoupled configuration. (a) Hourly resolved annual coupling efficiency. (b) 2D histogram of the coupling efficiency with regard to the total spectral irradiance impinging on the device. (c) Hourly resolved annual STH efficiency. (d) 2D histogram of the STH efficiency and the total spectral irradiance. (d) Hourly resolved annual hydrogen yield. (e) 2D histogram of the hydrogen yield and the total spectral irradiance.

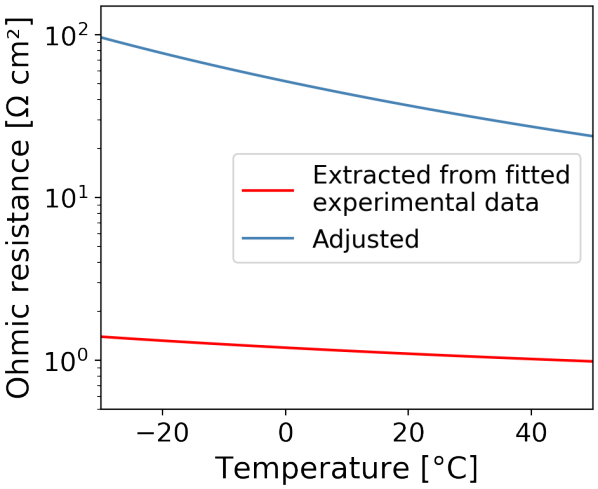

Fig. S10: Ohmic cell resistance of the electrolyzer as a function of its operating temperature. Red curve: Extracted resistance from the fitted set of temperature-dependent experimental IV curves (see Figure S1 and Table 2 in the manuscript). Blue curve: Resistance used for the reference modelling with a higher ohmic drop shown in the right bar pair of Figure 8 in the manuscript. To increase the resistance, a membrane activation energy $E_{\mathrm{a,\ mem}}$ of 11.4 kJ mol^{-1} was assumed.

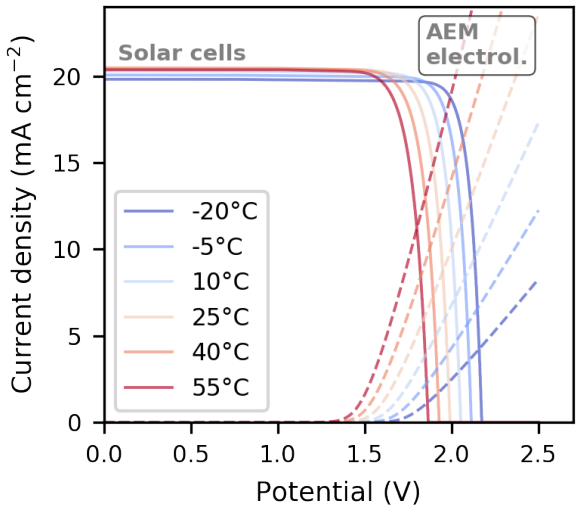

Fig. S11: Influence of the operating temperature on the IV characteristics of the AlGaAs//Si dual-junction and the AEM electrolyzer assuming the higher ohmic resistance as shown in Figure S10. The solar cell IV curves were modelled assuming AM1.5g illumination and an angle of incidence equal to 0°. An STH efficiency of 10.76% can be extracted for a temperature of 25°C.

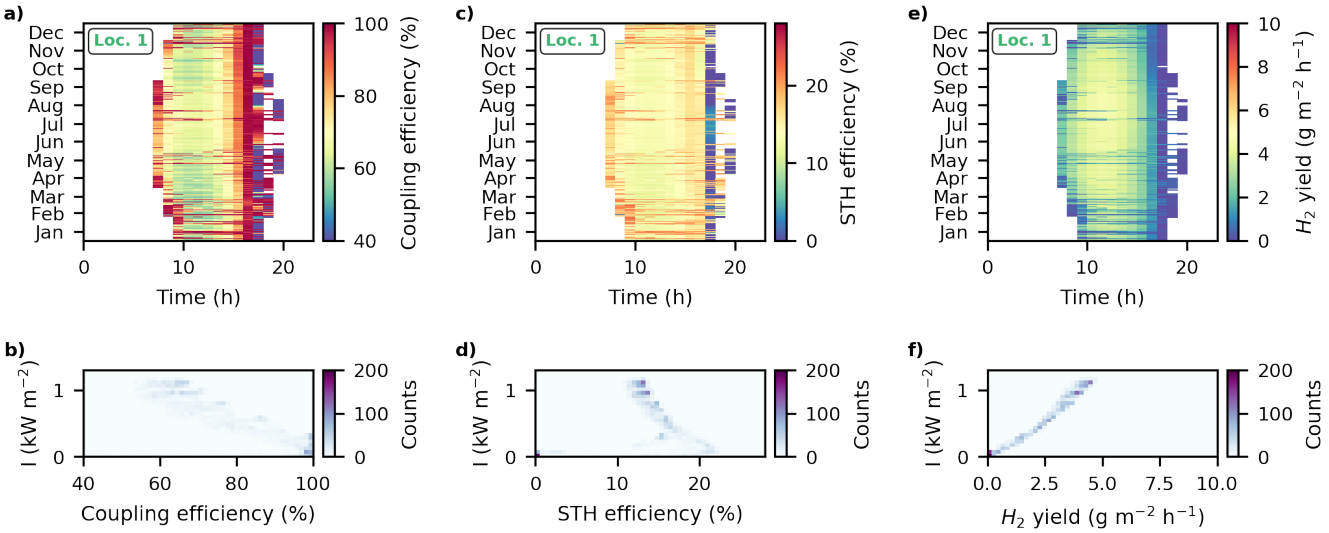

Fig. S12: Modelled climatic response of the solar water splitting device based on an AlGaAs//Si dual-junction and an AEM electrolyzer with a higher ohmic resistance (see Figure S10 and S11) for the location in southern California. (a) Hourly resolved annual coupling efficiency. (b)) 2D histogram of the coupling efficiency with regard to the total spectral irradiance impinging on the device. (c) Hourly resolved annual STH efficiency. (d) 2D histogram of the STH efficiency and the total spectral irradiance. (d) Hourly resolved annual hydrogen yield. (e) 2D histogram of the hydrogen yield and the total spectral irradiance.

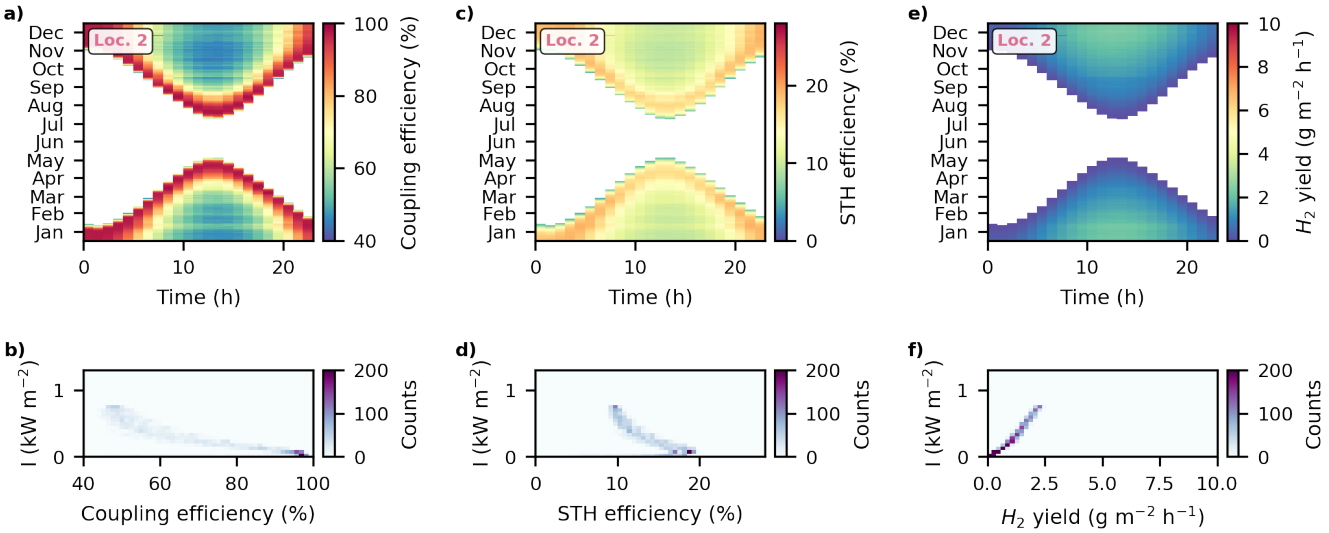

Fig. S13: Modelled climatic response of the solar water splitting device based on an AlGaAs//Si dual-junction and an AEM electrolyzer with a higher ohmic resistance (see Figure S10 and S11) for the location in Antarctica. (a) Hourly resolved annual coupling efficiency. (b) 2D histogram of the coupling efficiency with regard to the total spectral irradiance impinging on the device. (c) Hourly resolved annual STH efficiency. (d) 2D histogram of the STH efficiency and the total spectral irradiance. (d) Hourly resolved annual hydrogen yield. (e) 2D histogram of the hydrogen yield and the total spectral irradiance.

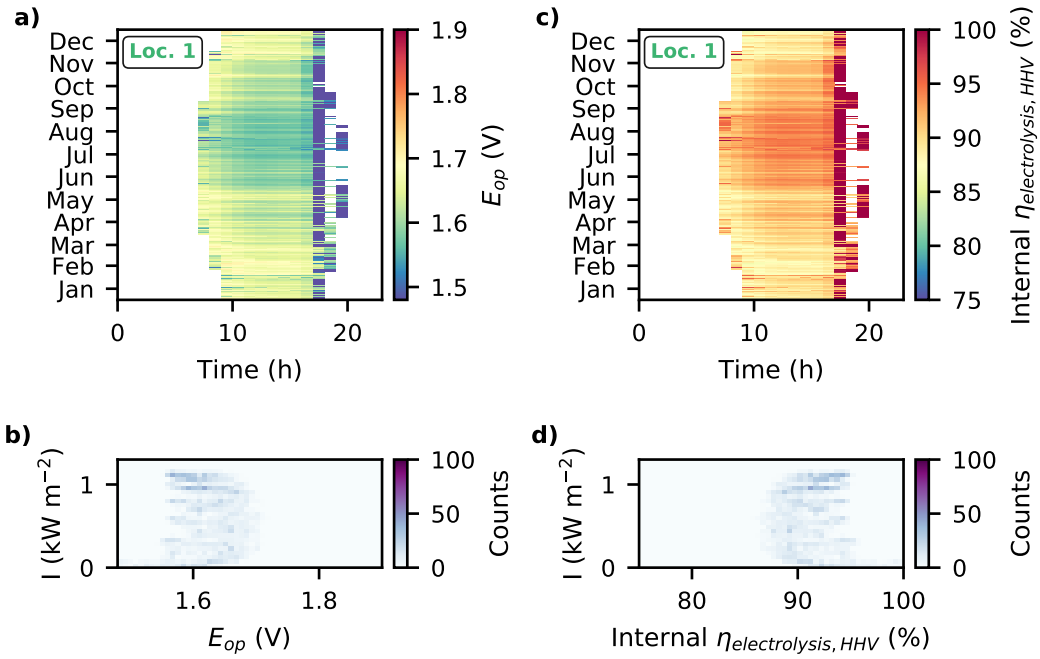

Fig. S14: Modelled climatic response with respect to the internal electrolysis efficiency of the solar water splitting device based on an AlGaAs//Si dual-junction and an AEM electrolyzer for the location in southern California. (a) Hourly resolved annual operation potential (E_{op}). (b) 2D histogram of the operation potential with regard to the total spectral irradiance impinging on the device. (c) Hourly resolved internal electrolysis efficiency according to the higher heating value ($\eta_{\mathrm{electrolysis,\ HHV}}$). (d) 2D histogram of the internal electrolysis efficiency with respect to the total spectral irradiance.

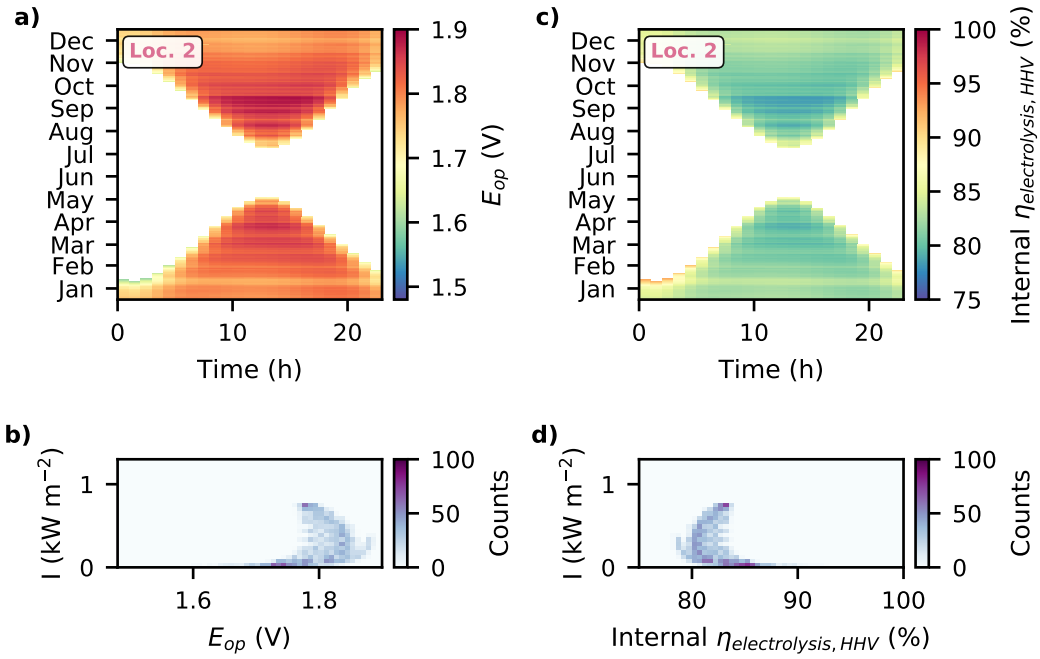

Fig. S15: Modelled climatic response with respect to the internal electrolysis efficiency of the solar water splitting device based on an AlGaAs//Si dual-junction and an AEM electrolyzer for the selected location in Antarctica. (a) Hourly resolved annual operation potential (E_{op}). (b) 2D histogram of the operation potential with regard to the total spectral irradiance impinging on the device. (c) Hourly resolved internal electrolysis efficiency according to the higher heating value ($\eta_{\mathrm{electrolysis,\ HHV}}$). (d) 2D histogram of the internal electrolysis efficiency with respect to the total spectral irradiance.

References

[1] I. Vincent, E.-C. Lee and H.-M. Kim, *Sci. Rep.*, 2021, **11**, 293.